Numerical study on the magnetohydrodynamics of an oscillatory flow under inductionless and core-side-layer approximations

J.A. Rizzo-Sierra and O.I. López-Hernández
Centro de Investigación en Ciencia Aplicada y Tecnología Avanzada. Instituto Politécnico Nacional,
Cerro Blanco # 141. Col. Colinas de Cimatario. 76090, Santiago de Querétaro, Querétaro, México.

A harmonically-driven, incompressible, electrically conducting, and viscous magnetohydrodynamic flow through a thin walled duct of rectangular cross section interacting with a uniform magnetic field transverse to its motion direction is numerically investigated. Spectral collocation method is used to solve the Navier-Stokes equation under the *inductionless* approximation for the magnetic field in the gradient formulation for the problem. Flow is considered fully developed in the direction perpendicular to the applied external magnetic field, laminar in regime, and feasible to be core-side-layer approximated. Flow structure and key features are numerically inquired regarding prospective alternating power generation applications in a liquid metal magnetodydrodynamic generator rectangular channel configuration. It is found that in the side layer and its vicinity the emerging flow structures/patterns depend mainly on the Hartmann number and oscillatory interaction parameter ratio. Formulation developed and tested with these calculations admits implementation of a generator configuration by means of load resistance attachment and walls conductivity optimization.

1. Introduction

Of central interest to this paper is the characterization of magnetohydrodynamic -MHD- flows occurring in ducts or channels interacting with moderate to high intensity magnetic fields. Apart from the physical interest of the subject, characterizing MHD flows is important in nuclear power generation (*e.g.*, liquid metal based cooling systems), alternative power generation/conversion (*e.g.*, liquid metal magnetohydrodynamic -LMMHD- electric generators/converters), and industrial liquid metal or conductive fluids transport and handling (*e.g.*, accelerators, pumps, flow meters). Generally, the analytical/theoretical treatment of MHD duct flow problems is difficult due to the coupling of fluid mechanics and electrodynamics equation. Because of that, exact analytical solutions are only available for relatively straightforward geometries subject to simple boundary conditions.

In response, over time a range of numerical techniques have been used to solve MHD duct flow problems, such as finite difference method (FDM) [30,31], finite element method (FEM) [3,15,16,24,25,32,35], finite volume method (FVM) [27], boundary element method (BEM) [4,5,14,20,29,33,34], and spectral collocation methods (SCM). SCM have been used in pure and applied mathematics [1,2,6-8,10,19,26], but also in MHD duct flow problems for the coupled steady case by Celik [9] and in the inductionless approach for the steady case as well by Cuevas *et al.* [13]. A combination of finite volume element method and spectral method is proposed in [27] by Shakeri *et al.* for the coupled velocity and magnetic field rectangular cross-section unsteady case, focusing on building and evaluating the method viability in terms of correctly combining the two techniques and establishing its validation respect to available

analytical solutions as well as numerical ones for Hartmann numbers of $O(\leq 10^2)$. In general, when applicable spectral collocation methods are found to be practical in terms of solid convergence towards solutions behavior and overall computational efficiency.

On oscillatory MHD duct flows precedent works include Mehmood *et al.*, who analytically investigated an oscillatory MHD porous filled duct flow linking the possible effects of heat and vibration transfer respect to boundary condition behavior [23]. Mandal developed a detailed analytical treatment of an oscillatory MHD flow through a rectangular cross-sectioned duct. His approach regards isolating walls parallel to the applied magnetic field (also referred as side or lateral walls) and thin arbitrary conducting walls perpendicular to the field (also referred as Hartmann walls) in [21] and thin arbitrary conducting side walls with perfectly conducting Hartmann walls in [22]. Additional examples of analytical treatment for MHD duct flow problems can be found in [11,17,18,28].

Here, the SCM based upon the work by Cuevas *et al.* for the steady MHD duct flow case [12,13] is used to develop a numerical study on a family of oscillatory flows potentially useful in alternating power generation. Formulation implemented allows considering both thin conducting side and Hartmann walls including insulating and perfectly conducting limit cases; but here we restrict ourselves to both thin side and Hartmann walls of equal conductivity under validity conditions for thin wall approximation as established in [12,13], case which isn't covered in [21,22]. This paper is distributed as follows. Problem is physically formulated in Sec. 2 below. In Sec. 3, a brief summary on the core-side-layer approximation and the employed spectral collocation numerical formulation is given. In Sec. 4, a comparison between our numer-

ical solution and an unrestricted analytical solution obtained for isolating side walls and perfectly conducting Hartmann walls ($C_L = 0$, $C_H \to \infty$) is presented. In Sec. 5, numerical results are presented and discussed in terms of dimensionless parameters defining the problem. Concluding remarks are given in Sec. 6. Finally, Appendix A gives further details on the obtention procedure of the analytical solution used in Sec. 4.

2. Physical formulation

Consider a harmonically-driven, incompressible, electrically conducting, laminar, completely developed, and viscous flow through a thin walled duct of rectangular cross section interacting with an uniform magnetic field transverse to its motion direction. Basic schematics in Fig. 1. Under these circumstances, functional dependence in Cartesian coordinates for spatial variables lies in y, z while t references time. $\vec{u} = u_x(y, z, t)\,\hat{e}_x$ defines the velocity field, where $\hat{e}_x$ is the unit vector in x direction. Conductivity of Hartmann walls (perpendicular to the applied magnetic field) is not necessarily the same as the one of the side walls (parallel to the applied magnetic field).

The velocity vector field is known by solving the Navier-Stokes equation:

$$\frac{\partial \vec{u}}{\partial t} + (\vec{u} \cdot \nabla)\,\vec{u} = -\frac{1}{\rho}\nabla p + \nu \nabla^2 \vec{u} + \frac{\vec{f}}{\rho} \qquad (1)$$

Where $p = p(x, t)$ and its gradient ∇p relate to the functional dependence of the pressure applied to the fluid, $\vec{B}$ is the applied homogeneous magnetic field, $\vec{f} = \vec{j} \times \vec{B}$ is the electromagnetic body force in the fluid, related to $\vec{j}$, the induced electric current, which in its turn is given by Ohm's law:

$$\vec{j} = \sigma\left(\vec{E} + \vec{u} \times \vec{B}\right) \qquad (2)$$

ρ is the fluid's volumetric mass density and ν its kinematic viscosity. If flow is assumed to be slow enough, the induced

FIGURE 1. Schematic of the problem.

magnetic field can be considered negligible compared to the externally imposed one. That constitutes the *inductionless* approximation, which can be expressed as $R_m = \nu_m \sigma u_0^* L \ll 1$. R_m is defined as the magnetic Reynolds number, a conventional MHD dimensionless parameter which represents the ratio between induction and diffusion of the magnetic field in a given situation. ν_m, σ, are the fluid's magnetic permeability and electrical conductivity while u_0^*, L are respectively one characteristic velocity and length for the problem. Moreover, if we reinterpret the *inductionless* approximation in terms of the much shorter time scale of magnetic field diffusion compared to that of velocity field variation, the quasi-stationary approximation yielding to $\vec{E} = -\nabla\phi$ becomes pertinent to the situation under consideration ($\phi = \phi(y, z, t)$ is the electrostatic potential). Using Ohm's law in the form $\vec{j} = \sigma\left(-\nabla\phi + \vec{u} \times \vec{B}\right)$, Eq. (2) turns into:

$$\vec{j} = \sigma\left(-\frac{\partial \phi}{\partial y}\hat{y} - \frac{\partial \phi}{\partial z}\hat{z} + uB_0\hat{z}\right) \qquad (3)$$

With it, the electromagnetic body force in Eq. (1) assumes the form:

$$\frac{\vec{f}}{\rho} = \sigma\left(-\frac{\partial \phi}{\partial y}\hat{y} - \frac{\partial \phi}{\partial z}\hat{z} + uB_0\hat{z}\right) \times B_0\hat{y} \qquad (4)$$

Replacing Eq. (4) into Eq. (1), one obtains:

$$\frac{\partial u}{\partial t} = -\frac{1}{\rho}\frac{\partial p}{\partial x} + \nu\left(\frac{\partial^2 u}{\partial y^2} + \frac{\partial^2 u}{\partial z^2}\right) - \frac{B_0}{\rho}j_z \qquad (5)$$

Proposing the adimensionalization given by $\tilde{B} = B/B_0 = 1$, $\tilde{u} = u/u_0^*$, $\tilde{t} = \omega t$, $\tilde{y} = y/L$, $\tilde{z} = z/L$, $\tilde{d} = d/L$, Eq. (5) conduces to:

$$N_\omega^{-1}\frac{\partial \tilde{u}}{\partial \tilde{t}} = -\frac{\partial \tilde{p}}{\partial \tilde{x}} + M^{-2}\left(\frac{\partial^2 \tilde{u}}{\partial \tilde{y}^2} + \frac{\partial^2 \tilde{u}}{\partial \tilde{z}^2}\right) - \tilde{j}_z \qquad (6)$$

The set of dimensionless parameters defining the problem is constituted by $M = B_0 L\sqrt{\sigma/\rho\nu}$, the Hartmann number, representing the ratio of electromagnetic to viscous forces in the problem, and $N_\omega = \sigma B_0^2/\rho\omega$, the oscillatory interaction parameter, representing the ratio of electromagnetic to inertial forces.

In order to solve Eq. (6) we propose variables to be harmonically dependent on time as follows:

$$\left\{\begin{array}{c} \tilde{u} \\ \tilde{\phi} \\ \tilde{\phi}_w \\ \tilde{p} \\ \frac{\partial \tilde{p}}{\partial \tilde{x}} \\ \tilde{j}_y \\ \tilde{j}_z \\ \tilde{j}_{yw} \\ \tilde{j}_{zw} \end{array}\right\} = \Re\left\{\left[\begin{array}{c} \tilde{u}_0(\tilde{y}, \tilde{z}) \\ \tilde{\phi}_0(\tilde{y}, \tilde{z}) \\ \tilde{\phi}_{0w}(\tilde{y}, \tilde{z}) \\ \tilde{p}_0(\tilde{x}) \\ \tilde{G} \\ \tilde{j}_{y0}(\tilde{y}, \tilde{z}) \\ \tilde{j}_{z0}(\tilde{y}, \tilde{z}) \\ \tilde{j}_{y0w}(\tilde{y}, \tilde{z}) \\ \tilde{j}_{z0w}(\tilde{y}, \tilde{z}) \end{array}\right]e^{i\tilde{t}}\right\} \qquad (7)$$
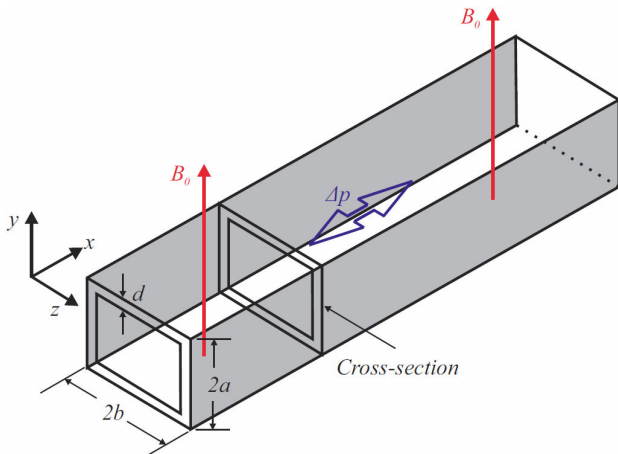
From top to bottom: velocity field, fluid region electric potential, wall region electric potential, pressure, gradient pressure, fluid region surface electric current density y component, fluid region surface electric current density z component, wall region surface electric current density y component, wall region surface electric current density z component. $\Re$ means taking the real part as physically meaningful. $\tilde{G}$ is the pressure gradient amplitude and $\partial \tilde{p}/\partial \tilde{x} = \left(1/\sigma B_0^2 u_0^*\right) \partial p/\partial x$ its adimensionalization equation. Replacing pertinent quantities into Eq. (6), one obtains a complex variable equation independent of time for the fluid region:

$$M^{-2}\left(\frac{\partial^2 \tilde{u}_0}{\partial \tilde{y}^2} + \frac{\partial^2 \tilde{u}_0}{\partial \tilde{z}^2}\right) - \tilde{j}_{z0} - iN_\omega^{-1}\tilde{u}_0 = \tilde{G} \quad (8)$$

Variables with tildes are dimensionless, and from now on, the notation will be dropped since dimensionless quantities will be assumed by implication. As stated, the solution for the velocity field will be the real part of $u = u_0\left(y, z\right) e^{it}$.

Charge conservation in the problem, expressed as $\nabla \cdot \vec{J} = 0$ implies that:

$$j_{yo} = -\frac{\partial \phi_0}{\partial y}, \qquad j_{zo} = -\frac{\partial \phi_0}{\partial z} + u_0 \quad (9)$$

$$\frac{\partial j_{y0}}{\partial y} + \frac{\partial j_{z0}}{\partial z} = 0 \quad (10)$$

$$j_{yow} = -\left(\frac{\sigma_H}{\sigma}\right)\frac{\partial \phi_{0w}}{\partial y}, \qquad j_{zow} = -\left(\frac{\sigma_L}{\sigma}\right)\frac{\partial \phi_{0w}}{\partial z} \quad (11)$$

$$\frac{\partial j_{y0w}}{\partial y} + \frac{\partial j_{z0w}}{\partial z} = 0 \quad (12)$$

As defined in Eq. (7), ϕ_0 and ϕ_{0w} are the electric potential spatial amplitudes within fluid and wall regions respectively. In their part, $\sigma_H/\sigma = C_H/d$ and $\sigma_L/\sigma = C_L/d$. C_H and C_L are defined as conductance ratios for Hartmann and side walls. It should be noticed that these quantities are dimensionless from definition. Consequently, the problem is defined by Eqs. (8) to (12), but further considerations must be made to complete its physical formulation. No initial conditions are required since presently we are not interested in the transient solution, so focus is put on boundary conditions.

Departing from considering symmetry in both y and z directions with $b = 1$ (shown in Fig. 2), a complete reformulation to the problem can be developed based on the
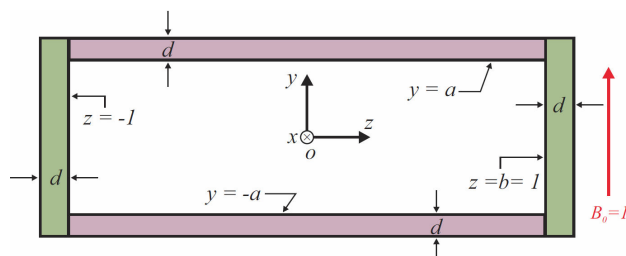
work by Cuevas [12] and Cuevas *et al.* [13] for the steady case, in order to advance the following steps into obtaining a solution. First, define pertinent to the case and proper hydrodynamic and electromagnetic boundary conditions within fluid, wall and outer regions. Second, exploiting the fact that the electric current is divergence free and two dimensional $(2-D)^i$ –see again Eqs. (9)-(12)–, propose for them properly defined fluid and wall regions electric current stream functions. Third, decouple the resulting equations within fluid region from those within wall and outer regions by forwarding a potential function in terms of both fluid region electric current stream function and electric potential and then applying for it the thin wall approximation, *i.e.*, regarding $d \ll 1$ and the medium around the duct (outer region) as fully isolating. d is the width of the duct walls, as shown in Fig. 2. These steps have the overall effect of rendering the system given by Eqs. (8)-(12) into a single variable within the fluid region^{ii}, *i.e.*, $F = F\left(y, z\right)$. Previous considerations conduce to the following set of equations and boundary conditions:

a) Fluid region governing equation.

$$M^{-2}\left(\frac{\partial^2 u_0}{\partial y^2} + \frac{\partial^2 u_0}{\partial z^2}\right) - \frac{\partial^2 F}{\partial y^2} - iN_\omega^{-1}u_0 = G \quad (13)$$

Where, given that $0 < y < a \wedge 0 < z < 1$:

$$u_0 = \frac{\partial^2 F}{\partial y^2} + \frac{\partial^2 F}{\partial z^2} \quad (14)$$

b) Boundary conditions. At $z = 0$:

$$\frac{\partial}{\partial z}\left(\frac{\partial^2 F}{\partial y^2} + \frac{\partial^2 F}{\partial z^2}\right) = 0, \qquad \frac{\partial F}{\partial z} = 0 \quad (15)$$

At $y = 0$:

$$\frac{\partial}{\partial y}\left(\frac{\partial^2 F}{\partial y^2} + \frac{\partial^2 F}{\partial z^2}\right) = 0, \qquad \frac{\partial F}{\partial y} = 0 \quad (16)$$

At $z = 1$:

$$\left(\frac{\partial^2 F}{\partial y^2} + \frac{\partial^2 F}{\partial z^2}\right) = 0, \qquad F + C_L\frac{\partial F}{\partial z} = 0 \quad (17)$$

At $y = a$:

$$\left(\frac{\partial^2 F}{\partial y^2} + \frac{\partial^2 F}{\partial z^2}\right) = 0$$

$$\frac{\partial F}{\partial y} - \left(C_H + M^{-1}\right)\frac{\partial^2 F}{\partial z^2} = M^{-1}\frac{\partial^2 F}{\partial y^2} \quad (18)$$

FIGURE 2. Duct dimensionless cross-section.

3. Core-side-layer approximation/numerical formulation

3.1. Approximation

The approximation entails flow solution by means of considering relevance restricted to core and side-layer region in an attempt to avoid excessive computational costs. Supposing M sufficiently large, flow in Hartmann layers and duct corners can be progressively neglected. But Hartmann layers are still regarded as return paths for the current, which implies effectively accounting for the limit case $C_H = C_L \to 0$. Further details for the steady case in [12,13].

Operating as described on governing Eq. (8) one reaches:

$$\frac{\partial^2 F}{\partial y^2} - M^{-2}\frac{\partial^2 u_0}{\partial z^2} + iN_\omega^{-1}u_0 = G \qquad (19)$$

Using $u_0 = \partial^2 F/\partial y^2 + \partial^2 F/\partial z^2$, and neglecting terms less than $O\left(M^{-1}\right)$:

$$u_0 = \left(\frac{1 - iN_\omega^{-1}}{1 + N_\omega^{-2}}\right)\left(G + \frac{\partial^2 F}{\partial z^2}\right) \qquad (20)$$

Which rewrites governing Eq. (19) into:

$$\frac{\partial^2 F}{\partial y^2} - M^{-2}\frac{\partial^4 F}{\partial z^4} + iN_\omega^{-1}\frac{\partial^2 F}{\partial z^2} = G\left(1 - iN_\omega^{-1}\right) \qquad (21)$$

In its turn, neglecting terms less than $O\left(M^{-1}\right)$ on the boundary conditions Eqs. (15)-(18) conduces to:
At $z = 0$:

$$\frac{\partial}{\partial z}\left(u_0\right) = 0 \Longrightarrow \frac{\partial^3 F}{\partial z^3} = 0, \qquad \frac{\partial F}{\partial z} = 0 \qquad (22)$$

At $y = 0$:

$$\frac{\partial}{\partial y}\left(u_0\right) = 0 \Longrightarrow \frac{\partial^3 F}{\partial y \partial z^2} = 0, \qquad \frac{\partial F}{\partial y} = 0 \qquad (23)$$

At $z = 1$:

$$G + \frac{\partial^2 F}{\partial z^2} = 0, \qquad F + C_L\frac{\partial F}{\partial z} = 0 \qquad (24)$$

At $y = a$:

$$\frac{\partial F}{\partial y} - \left(C_H + M^{-1}\right)\frac{\partial^2 F}{\partial z^2} = M^{-1}G \qquad (25)$$

These finally complete the specific formulation of our problem within the core-side-layer approximation.

In addition to what is conditioned by means of Eqs. (19) to (25), the physical formulation must also take into account the dimensionless volumetric flow conservation condition in terms of the averaged velocity amplitude (u_0):

$$\int\limits_0^a \int\limits_0^1 u_0 dy dz = a \qquad (26)$$

Equation (26) comes from

$$\int_S \overrightarrow{u_0} \cdot \overrightarrow{ds} = \int_0^a \int_0^1 u_0 dy dz = a,$$

since a is simultaneously the duct cross section dimensionless area and aspect ratio. Because the spatial average of u_0 is

$$\langle u_0 \rangle = \int \overrightarrow{u_0} \cdot \overrightarrow{ds} \Big/ \int_S ds,$$

in order to normalize u respect to it one has:

$$u_n = \frac{u\left(y, z, t\right)}{\langle u_0 \rangle} = a\frac{u_0\left(y, z\right)e^{it}}{\int\limits_0^a \int\limits_0^1 u_0 dy dz} \qquad (27)$$

3.2. Numerical formulation

In order to solve Eqs. (21)-(25) by means of the spectral collocation method, a function $F = F\left(y, z\right)$ satisfying the boundary conditions is proposed as a finite series of even Chebyshev polynomials ($T_{2m}\left(y/a\right)$, and $T_{2n}\left(z\right)$):

$$F = \sum_{m=0}^{N_y}\sum_{n=0}^{N_z} A_{mn}T_{2m}\left(\frac{y}{a}\right)T_{2n}\left(z\right) \qquad (28)$$

Variables to determine are the complex coefficients A_{mn}. N_y and N_z are the number of terms taken along y and z coordinates respectively. Use of he Gauss-Lobatto collocation points set is convenient because it yields the appropriate numerical resolution for the boundary layers by concentrating the points near the walls (in this case the side wall). The unknown coefficients can be considered as a vector $\beta\left(AJ\right) = A_{mn}$, and the algebraic system of simultaneous equations can be expressed as:

$$\sum_{AJ=1}^{N_T}\alpha_{PJ\times AJ}\beta_{AJ} = \gamma_{PJ} \qquad (29)$$

Where $AJ = m\left(N_z + 1\right) + n + 1$, $1 \le PJ \wedge AJ \le N_T$, and $N_T = \left(N_y + 1\right)\left(N_z + 1\right)$. Elements of matrix $\alpha_{PJ\times AJ}$ and known vector $\gamma_{(PJ)}$ are obtained by replacing Eq. (28) into Eqs. (21)-(25). Explicitly, into governing Eq. (21):

$$\sum_{m=0}^{N_y}\sum_{n=0}^{N_z}\left[\frac{1}{a^2}\frac{\partial^2 T_{2m}\left(\frac{y}{a}\right)}{\partial y^2}T_{2n}\left(z\right) - M^{-2}T_{2m}\left(\frac{y}{a}\right)\frac{\partial^4 T_{2n}\left(z\right)}{\partial z^4} + iN_\omega^{-1}T_{2m}\left(\frac{y}{a}\right)\frac{\partial^2 T_{2n}\left(z\right)}{\partial z^2}\right]A_{mn} = G\left(1 - iN_\omega^{-1}\right) \qquad (30)$$

Into Eqs. (22) and (23), boundary conditions at $z = 0$ and $y = 0$ are identically satisfied, so no equations are generated. Into Eq. (24), the hydrodynamic boundary condition at $z = 1$ results:

$$\sum_{m=0}^{N_y} \sum_{n=0}^{N_z} \left[\frac{4n^2}{3} \left(4n^2 - 1\right) T_{2m} \left(\frac{y}{a}\right) \right] A_{mn} = -G \quad (31)$$

Electromagnetic boundary condition at $z = 1$ results:

$$\sum_{m=0}^{N_y} \sum_{n=0}^{N_z} \left[\left(1 + 4n^2 C_L\right) T_{2m} \left(\frac{y}{a}\right) \right] A_{mn} = 0 \quad (32)$$

Into Eq. (25), the electromagnetic boundary condition at $y = a$ results:

$$\sum_{m=0}^{N_y} \sum_{n=0}^{N_z} \left[\frac{4m^2}{a} T_{2n}(z) - \left(C_H + M^{-1}\right) \frac{\partial^2 T_{2n}(z)}{\partial z^2} \right] A_{mn} = M^{-1} G \quad (33)$$

The system of linear simultaneous equations in the variables A_{mn} given by Eqs. (30)-(33) can be solved by Gauss-Jordan elimination.

4.   Analytical vs. numerical comparison

Numerical calculations are validated if they can reproduce established analytical results, in this case, for velocity profiles. An instance of validation is provided by comparing numerical results with analytical solutions for the oscillatory flow case, as shown in Fig. 3. This was performed by obtaining an analytical solution for isolating side walls and perfectly conducting Hartmann walls ($C_L \to 0$, $C_H \to \infty$) at a moderate Hartmann number, case which was also treated in [22] but restricted there to an asymptotic approximation for large Hartmann numbers ($M \gg 1$). The unrestricted analytical solution was obtained by means of the separation of variables technique in the potential formulation for the problem (ϕ-formulation), see Appendix A for details.
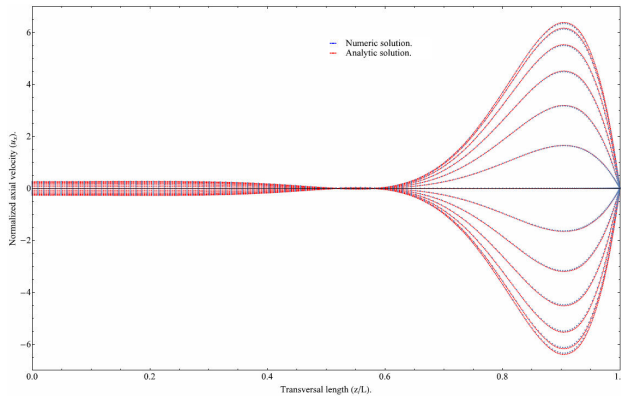
Solution reads:

FIGURE 3. Collocation vs. analytical oscillatory solutions for a duct flow with moderate Hartmann number (M) and high interaction parameter (N_ω). $M = 10^2$, $N_\omega = 10^6$, and $t = 0 - \pi \, Rads$ in increments of $\pi/12 \, Rads$. $C_L \to 0$, $C_L \to \infty$, $a = 1$. Profiles at plane $y = 0$.

$$u(y, z, t) = \sum_{n=0}^{\infty} \left(\frac{\delta e^{-\frac{y(\sqrt{\epsilon_1} + \sqrt{\epsilon_2})}{\sqrt{2}}}}{8\pi\gamma(2n+1)\epsilon} \left(e^{\zeta_1 y} \left(4\epsilon e^{\zeta_2 y} \left((2n+1)\pi\right)^2 + \epsilon_1 \left(\left((2n+1)\pi\right)^2 - 2\epsilon_2 \right) \left(e^{\sqrt{2}y\sqrt{\epsilon_2}} + 1\right) Sech(a\zeta_2) \right) \right) \right.$$

$$\left. - \epsilon_2 e^{\zeta_2 y} \left(\left((2n+1)\pi\right)^2 - 2\epsilon_1 \right) \left(e^{\sqrt{2}y\sqrt{\epsilon_1}} + 1\right) Sech(a\zeta_1) \right) \cos(\alpha_n z) e^{i\omega t} \quad (34)$$

u being the magnitude of the velocity field, with the following dimensionless parameters/constants: $\eta = 1 + iN_\omega^{-1}$, $\beta = \eta M^2 + \alpha_n^2$, $\gamma = (1 - \eta)M^2\alpha_n^2 - \alpha_n^4$, $\delta = GM^2 a_n \alpha_n$, $\epsilon = \sqrt{\beta^2 + 4\gamma}$, $\epsilon_1 = \beta - \epsilon$, $\epsilon_2 = \beta + \epsilon$, $\zeta_1 = \sqrt{\epsilon_1}/\sqrt{2}$, and $\zeta_2 = \sqrt{\epsilon_2}/\sqrt{2}$.

5.   Results

Once found that numerical results are close to analytical results, a picture of the flow dynamics and structure is drawn by a parametric study in terms of Hartmann number M, oscillatory interaction parameter N_ω, and wall conductance ratio value $C_H = C_L = C$. Emphasis was put on Hartmann numbers as high as possible because they are characteristic

of strong applied magnetic fields, paramount in electric generation applications. The range of the oscillatory interaction parameter was chosen primarily due to our interest in the flow at the low frequencies case having in mind liquid metal MHD generators. Finally, regarding C, values 0.0, 0.001, 0.01, and 0.05 were chosen due to interest in taking into account the transition from thin conducting to insulating wall case.

The number of collocation points to use for the obtention of a numerically stable collocation solution is a subtle topic. Generally speaking, the oscillatory case on this particular subject is a self contained matter of inquiry since it varies in terms of both increasing M and M/N_ω. A picture of the situation is grasped with Table I, filled with values of

TABLE I. M/N_ω, NY, and NZ for the set of numerical experiments performed.

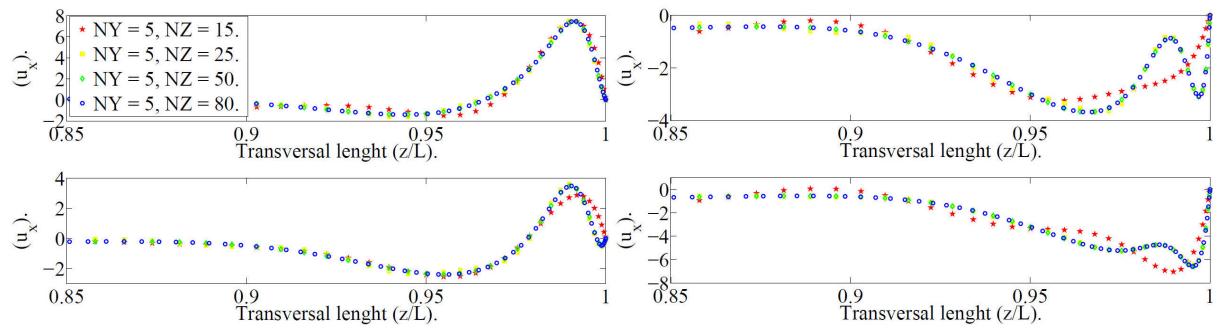| $N_\omega \downarrow$, $M \rightarrow$	10^2	10^3	10^4	10^5
10^3	$10^{-1}, 5, 55.$	$10^0, 5, 65.$	$10^1, 5, 75.$	$10^2, 5, 240.$
10^4	$10^{-2}, 5, 55.$	$10^{-1}, 5, 65.$	$10^0, 5, 75.$	$10^1, 5, 240.$
10^5	$10^{-3}, 5, 55.$	$10^{-2}, 5, 65.$	$10^{-1}, 5, 75.$	$10^0, 5, 240.$
10^6	$10^{-4}, 5, 55.$	$10^{-3}, 5, 65.$	$10^{-2}, 5, 75.$	$10^{-1}, 5, 240.$
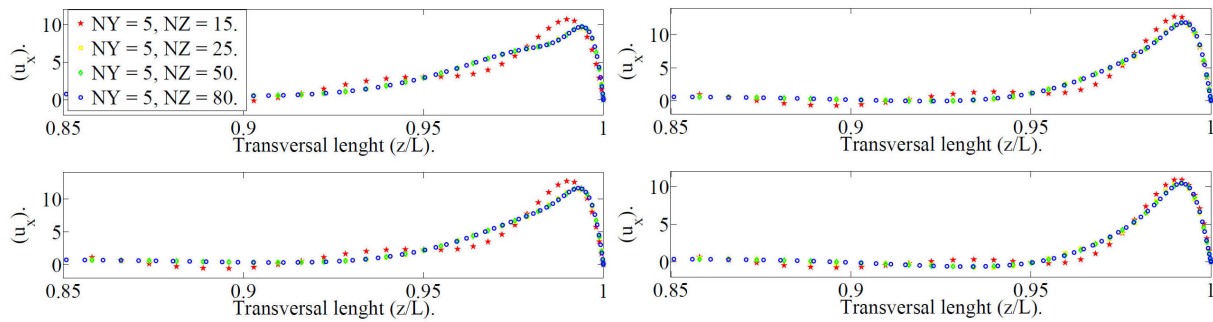
FIGURE 4. Numerical solution respect to collocation/graph parameters. $C = 0.05$, $N_\omega = 10^3$, $M = 10^4$, $M/N_\omega = 10$. Left: $t = 0$ $(top) \wedge \pi/8$ $(bottom)$ $Rads$. Right: $t = 2\pi/8$ $(top) \wedge 3\pi/8$ $(bottom)$ $Rads$. Profiles at plane $y = 0$.

FIGURE 5. Numerical solution respect to collocation/graph parameters. $C = 0.05$, $N_\omega = 10^3$, $M = 10^4$, $M/N_\omega = 10$. Left: $t = 4\pi/8$ $(top) \wedge 5\pi/8$ $(bottom)$ $Rads$. Right: $t = 6\pi/8$ $(top) \wedge 7\pi/8$ $(bottom)$ $Rads$. Profiles at plane $y = 0$.

M/N_ω, NY, and NZ. The last two register values above which the collocation oscillatory solution was found to be stable up to at least three significant figures within the ranges checked.

In order to illustrate the oscillatory solution behavior respect to the number of collocation and graph points, Figs. 4 and 5 show four different sets of collocation/graph parameters for $C = 0.05$, $N_\omega = 10^3$, $M = 10^4$, $t = 0 - \pi$ Rads. As depicted, while time elapses the solution could vary greatly before stability with increasing values of set parameters is attained. From the figures it can be seen that the region of interest is the final 10-5% of the duct's transversal length where differences between solutions are clearly noticeable, specially at Fig. 5 (right, top). As can be distinguished as well, interpolation solutions with $NZ = 15$ and 25 are not stable yet, which is more apparent at Fig. 5 (left). In sharp contrast, solutions with $NZ = 50$ and 80 have ceased to oscillate between adjacent collocation points. This advices to

carefully place collocation/graph parameters since flow structure could be entirely missed by not employing enough collocation points, for example, Fig. 5 (left, bottom) and 5 (right, top). No other examples are shown here.

In summary, what was observed advices us to carefully establish collocation parameters when searching for a numeric solution since flow structure patterns could be entirely missed in the side wall layer by not employing enough collocation points. The analysis on the influence of collocation parameters over the solution obtained also showed that flow structure patterns in the side wall layer could get a little more complex when compared to the steady case once MHD effects are established with its characteristic M-shaped profiles, back-flows and overshoots as illustrated and discussed in [12,13]. Main observations are that flow structure in the oscillatory collocation situation for the side wall layer depends not only on increasing M but on increasing M/N_ω ratio. As M/N_ω increased, the flow bulk gets progressively located
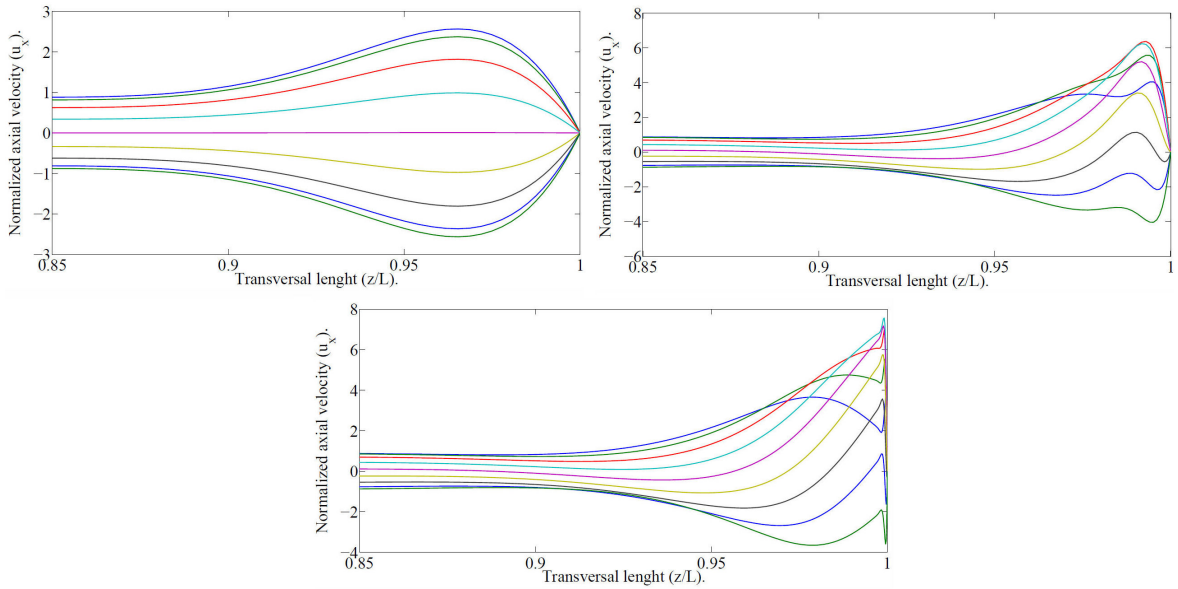
FIGURE 6. Velocity profiles at plane $y = 0$, $C = 0.01$. Top left: $N_\omega = 10^5$, $M = 10^3$; $^M/_{N_\omega} = 10^{-2}$. Top right: $N_\omega = 10^3$, $M = 10^4$; $^M/_{N_\omega} = 10$. Bottom: $N_\omega = 10^3$, $M = 10^5$; $^M/_{N_\omega} = 10^2$.
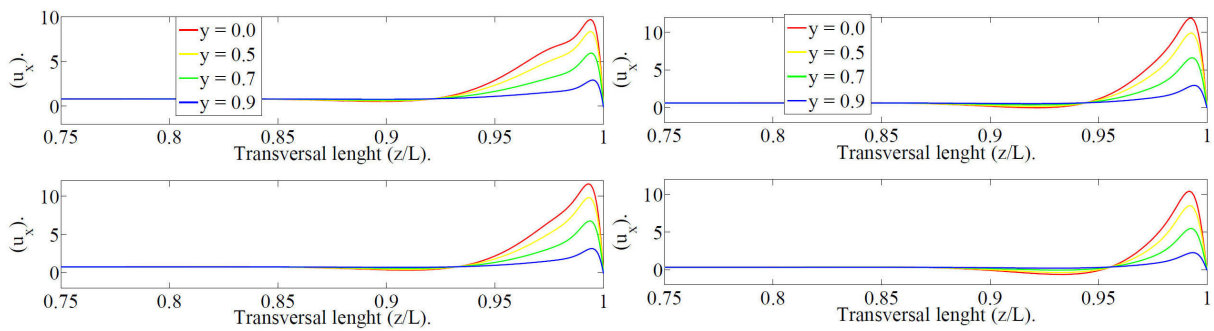

FIGURA 7. Oscillatory collocation solution velocity profiles at different planes/time-step evolution. $C = 0.05$, $N_\omega = 10^3$, $M = 10^4$; $^M/_{N_\omega} = 10^1$. Left: $t = 0$ $(top) \wedge {}^\pi/_8$ $(bottom)$ $Rads$. Right: $t = {}^{2\pi}/_8$ $(top) \wedge {}^{3\pi}/_8$ $(bottom)$ $Rads$.

for the most part into the last 15-10% of the duct transverse length, while simultaneously flow structure showed increasing complexity in terms of the emergence of clearly differentiated flow patterns. Figure 6 attempts to illustrate these remarks by showing velocity profiles for the side wall layer over a semi-period ($t = 0 - \pi\,Rads$) divided in increments of $\pi/8\,Rads$ for three cases of increasing $^M/_{N_\omega}$ within the parametric ranges solved. In Fig. 6 (top left) with $^M/_{N_\omega} = 10^{-2}$, profiles have an smooth M-shaped contour but they progressively transition into a little more complicated shape in Figs. 6 (top right) and (bottom), with $^M/_{N_\omega} = 10$ and 10^2 respectively. Notice also how from Fig. 6 (top left) to 6 (bottom) flow structure keeps getting closer and closer to $z = 1$.

Other aspects in need of illustration are the behavior of the oscillatory collocation solution respect to the plane of visualization longitudinal to the externally applied magnetic field and the time-step evolution of velocity profiles. Figures 7 and 8 show the behavior of the velocity profiles with respect to the plane of visualization while simultaneously present a grasp on the profiles time-step evolution for one example

with $M = 10^4$, in order to show how flow structure develops for this relatively high Hartmann number. Other numerically calculated cases are not shown due to space constraints. Profiles are shown over a semi-period divided in increments of $\pi/8\,Rads$, but the one corresponding to $t = \pi\,Rads$ is not shown due to its symmetry with the profile at $t = 0\,Rads$. At $t = 0\,Rads$, the velocity profile time-step evolution begins but not at its maximum normalized value for the time set solved, which is reached at Fig. 7 (left, bottom). Right at a quarter of the semi-period ($t = \pi/4\,Rads$) the profile begins to reverse its direction, while flow structure remains pretty much the same, resembling an smoothly serrated M-shape, with the apparition of a little bit of back-flow as noticeable at Fig. 7 (right, bottom). That initial back-flow keeps increasing along the new flow direction, while simultaneously the initial overshoot in the same figure keeps diminishing, as shown in Fig. 8 (right, top) and (right, bottom). This continues to happen until flow structure develops into what is shown in Fig. 8 (right, bottom); two valleys and two peaks in the negative direction, one of each more pronounced than the other towers
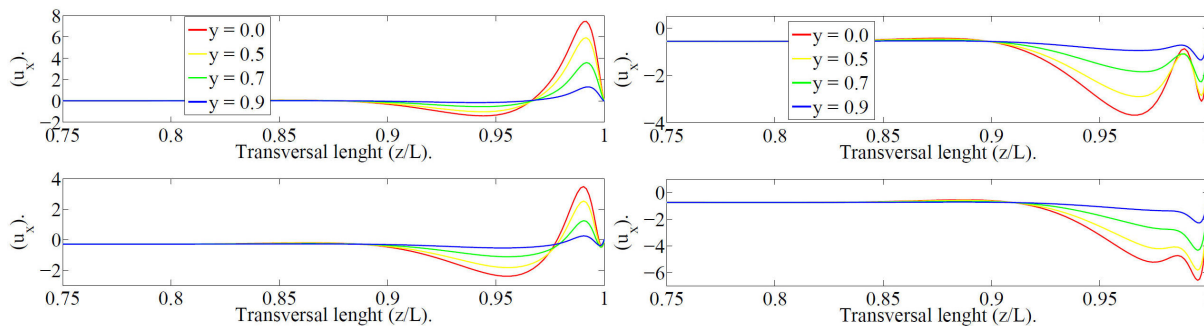
FIGURA 8. Oscillatory collocation solution velocity profiles at different planes/time-step evolution. $C = 0.05$, $N_\omega = 10^3$, $M = 10^4$; $M/N_\omega = 10^1$. Left: $t = 4\pi/8 \ (top) \wedge 5\pi/8 \ (bottom) \ Rads$. Right: $t = 6\pi/8 \ (top) \wedge 7\pi/8 \ (bottom) \ Rads$.
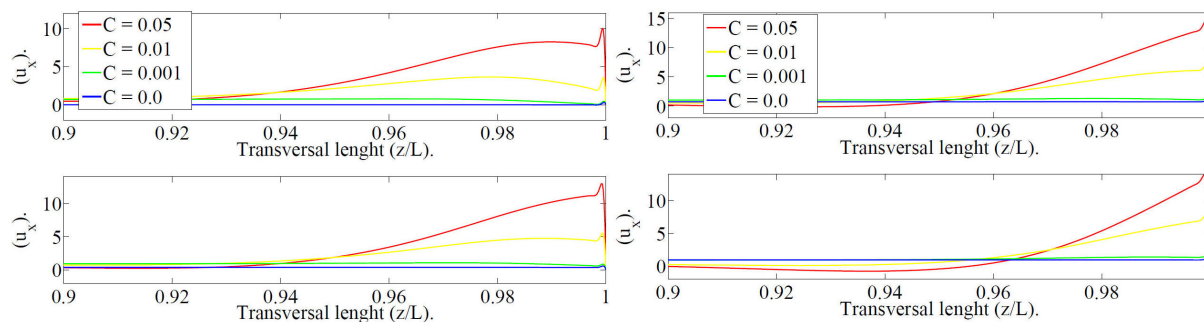

FIGURA 9. Oscillatory collocation solution respect to the wall conductance parameter/time-step evolution. Profiles at plane $y = 0$. $N_\omega = 10^3$, $M = 10^5$, $M/N_\omega = 10^2$. Left: $t = 0 \ (top) \wedge \pi/8 \ (bottom) \ Rads$. Right: $t = 2\pi/8 \ (top) \wedge 3\pi/8 \ (bottom) \ Rads$.
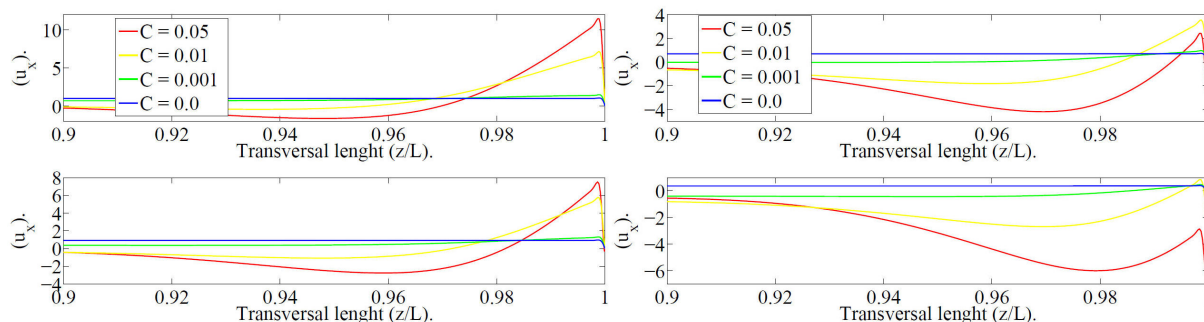

FIGURA 10. Oscillatory collocation solution respect to the wall conductance parameter/time-step evolution. Profiles at plane $y = 0$. $N_\omega = 10^3$, $M = 10^5$, $M/N_\omega = 10^2$. Left: $t = 4\pi/8 \ (top) \wedge 5\pi/8 \ (bottom) \ Rads$. Right: $t = 6\pi/8 \ (top) \wedge 7\pi/8 \ (bottom) \ Rads$.

towards the duct boundary. From this point on, flow continues to evolve to eventually form again what was described as an smoothly serrated M-shape of Fig. 7 (left, top) but in the opposite direction. Then the cycle resets the sequence in the symmetric second semi-period not shown here. All along Figs. 7 and 8 also show the behavior of the oscillatory collocation solution velocity profiles at different visualization planes ($0 < y < a$), presenting the correct differentiation between them regarding their individual relative proximity to boundary $y = a$ and its non slip condition. As shown, profiles at different planes present the same basic shape but more and more attenuated as they get closer to the boundary.

Figures 9 and 10 present both the behavior of the oscillatory collocation solution respect to the wall conductance parameter (C) and its time-step evolution. No other numeri-

cally calculated cases are shown because of space constraints. From Fig. 9 (left, top) to 10 (left, bottom), profiles with $C \neq 0$ exhibit a basic structure shape through almost the entire semi-period, which in this particular case of parameters can be described as an smoothed M-shape with an small peak towards the boundary $z = 1$; peak which gets smaller with diminishing values of C. That basic shape does not change dramatically for each value of C but for the appearance of a progressive back-flow (Fig. 9 (right, bottom) to Fig. 10 (left, top)), that for the particular case of $C = 0.001$ can be only appreciated by the end of the semi-period (Fig. 10 right, bottom), and the formation of a second valley or back-flow when the initial peak towards the boundary reverses its direction, which can be appreciated in incipience in Fig. 10 (right, top). Notice how all along for profiles with $C = 0$ the case
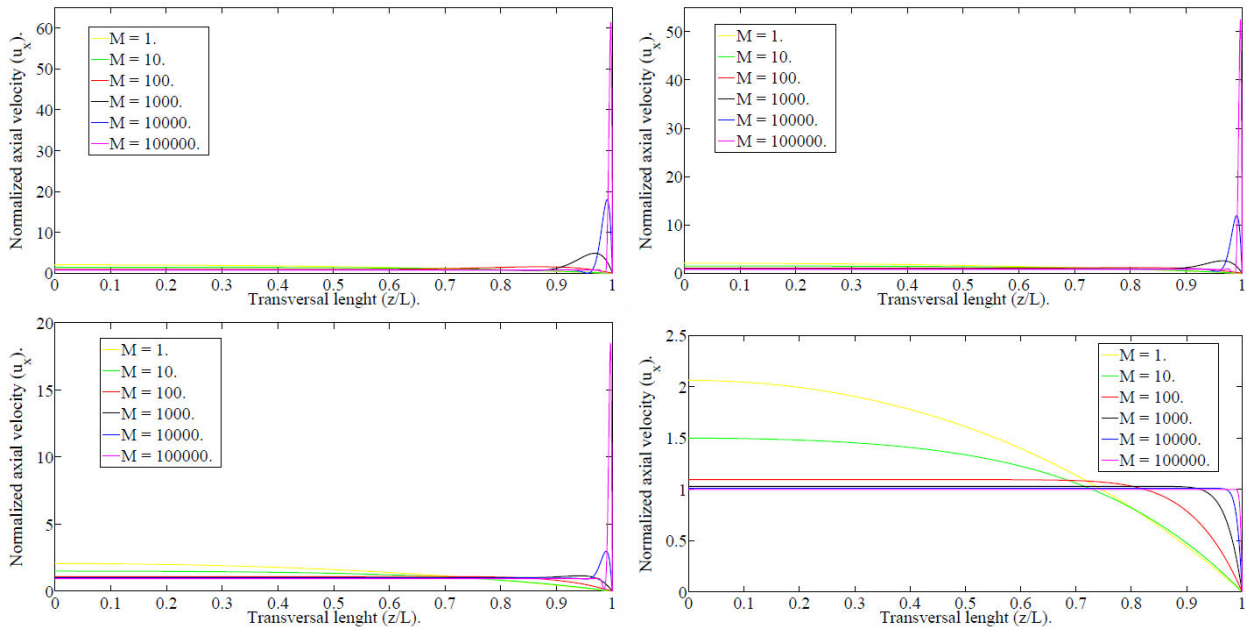
FIGURA 11. Oscillatory collocation solution respect to the Hartmann number. $N_\omega = 10^6$, $t = 0$ $Rads$. Profiles at plane $y = 0$. Top left: $C = 0.05$. Top right: $C = 0.01$. Bottom left: $C = 0.001$. Bottom right: $C = 0$.
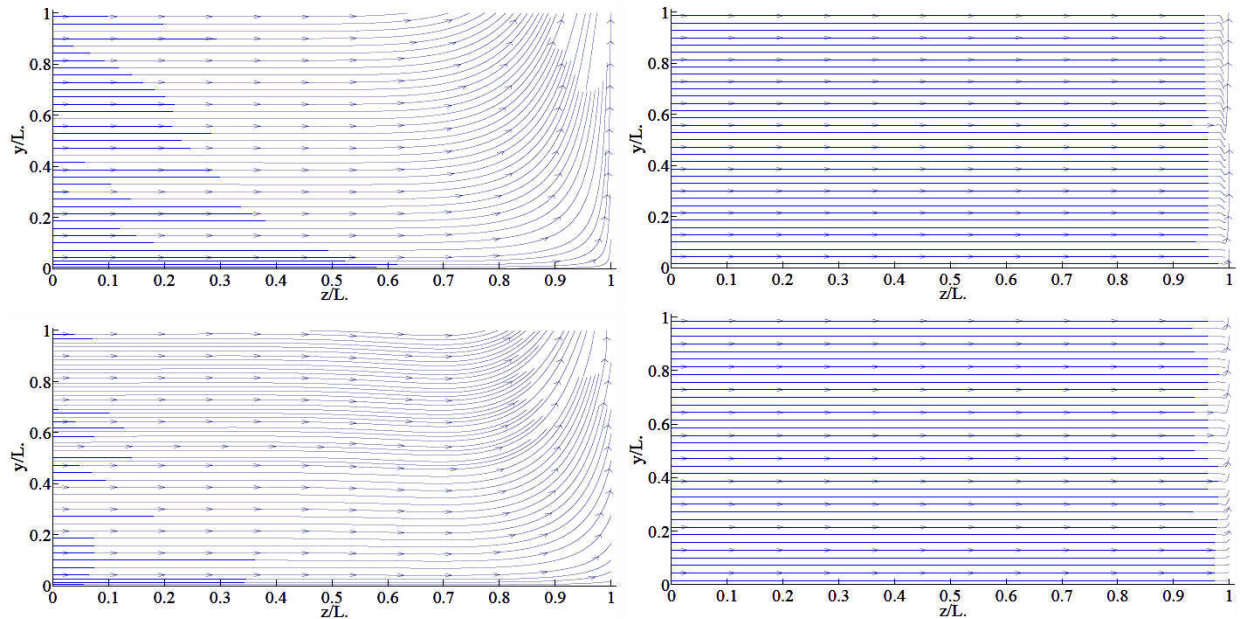

FIGURA 12. Electric current surface density ($\vec{j}$) respect to the Hartmann number. $N_\omega = 10^6$, $t = \pi\,Rads$. Top left: $C = 0.001$, $M = 10^2$. Top right: $C = 0.001$, $M = 10^5$. Bottom left: $C = 0.05$, $M = 10^2$. Bottom right: $C = 0.05$, $M = 10^5$.

the case is different since they present no back-flow and the small peak towards the boundary at $z = 1$ is much more less pronounced. This kind of flow structure can be described as slug-like.

Another characteristic to consider is the flow behavior respect to varying Hartmann number value (M). This is illustrated in Fig. 11. Although here is only shown $t = 0$ $Rads$, for each of the time-steps numerically solved figures match the features described in [12,13] for the steady case. Notice

particularly how for increasing M the peak velocity value also increases sharply, while on its part the side layer thickness decreases simultaneously as expected. For $M = 10^3$ and $C \neq 0$ in Fig. 11 (except right, bottom), the peak velocity value is around 10% of its value with $M = 10^5$ due to the side layer velocity being $O(M^{1/2})$; while correspondingly the side layer thickness being $O(M^{-1/2})$. As for $C = 0$, since in that case the induced electric currents close totally within the fluid and through the Hartmann layers, that circumstance

seriously dampens the velocity overshoots and the side layer velocity results now of $O(1)$, as shown in Fig. 11 (right, bottom).

It's also interesting for the scope of this paper to briefly inquire on the induced electric current surface density ($\overrightarrow{j}$) distribution over the duct, which in the present configuration would be equivalent to an open circuit liquid-metal generator with a single wall conductance parameter, by no means an efficient setup for electric generation. A more suitable generator-like setup would be one considering $C_H = 0$, $C_L \to \infty$, with the attachment of a load resistance between the side walls. Mentioned inquiry was performed in Fig. 12 for wall conductance parameters (C) values of 0.001 and 0.05. It is noticeable how as $C \sim 0$ and M increases, more of the electric current lines close within the increasingly thinner side and Hartmann layers in the fluid region, the latter we must remember are not solved and therefore not shown in the present approximation. Extreme cases for this situation in the parameters shown are apparent in Fig. 12 (top left) and Fig. 12 (bottom right). For a given $C \neq 0$ value, the trend to notice is pretty much the same in terms that with increasing M the side and Hartmann layers for electric current return get thinner while the closing of the electric current lines within the conducting walls is augmented for both side and Hartmann walls (Figs. 12 (bottom, left) and 12 (bottom, right)).

As illustrated, relevant parameters to take into account regarding flow features and behavior with a given conductance parameter value C are M, N_ω, and its ratio (M/N_ω). Numerical solutions for the oscillatory case were validated by comparison with an analytical oscillatory solution. Behavior and features of the numerical collocation oscillatory solution respect to several parameters were inquired as follows: varying number of collocation points (NZ being the relevant parameter due to the core-side layer approximation employed) and time-step profile evolution, see Figs. 4 and 5; varying M/N_ω ratio, see Fig. 6; different planes of visualization and time-step profile evolution, see Figs. 7 and 8; different wall conductance parameter values (C) and time-step velocity profile evolution, see Figs. 9 and 10; varying Hartmann number value (M), see Fig. 11; and electric current surface density respect to Hartmann number, see Fig. 12.

6. Conclusion

A harmonically-driven, incompressible, electrically conducting, laminar, completely developed, and viscous flow through a thin walled duct of rectangular cross section interacting with a uniform magnetic field tranverse to its motion (axial) direction was numerically investigated under the inductionless approach. Flow was core-side-layer approximated and thin conducting boundary conditions at top/side (Hartmann/lateral) walls were proposed in order to include the insulating case. In this approximation the Hartmann layers are considered merely as return paths for the electrical currents and aren't numerically solved. Concordance between oscillatory analytical and numerical calculations was established

revisiting a classic analytic asymptotic solution restricted to large Hartmann numbers in [22]. Several features of the oscillatory flow were explored in a parametric range of interest for MHD alternating power generation. The system described represents a liquid metal magnetohydrodynamic generator functioning in an unoptimized open circuit configuration. Influence over the velocity profiles of parameters such as wall conductance ratio (C), Hartmann number (M), and oscillatory interaction parameter (N_ω) was studied. It was found that in the side layer and its vicinity emerging flow structures/patterns depend mainly on the Hartmann number and oscillatory interaction parameter ratio (M/N_ω). Increasing values of M/N_ω are associated to more complex (in terms of generally more serrated in shape) flow structures/patterns towards the boundary in the velocity profiles. These calculations set the first step towards the numerical investigation on the performance of a cartesian-symmetric liquid metal MHD generator through the calculation of its isotropic efficiency. A suitable generator-like setup would consider $C_H = 0$, $C_L \to \infty$ as first approximation and the attachment of a load resistance to the side walls, things which are within the feasibility of the formulation developed here.

Appendix

A. Analytical details

Equation to be solved is:

$$\frac{\partial \overrightarrow{u}}{\partial t} + (\overrightarrow{u} \cdot \nabla) \overrightarrow{u} = -\frac{1}{\rho}\nabla p + \nu \nabla^2 \overrightarrow{u} + \frac{\overrightarrow{j} \times \overrightarrow{B}}{\rho} \quad \text{(A.1)}$$

Considering

$$\overrightarrow{u} = \overrightarrow{u}(y, z, t)\hat{e}_x, \quad \phi = \phi(y, z, t), \quad \overrightarrow{B} = \overrightarrow{B_0} + \overrightarrow{b} \approx \overrightarrow{B_0}$$

(inductionless approximation), $\overrightarrow{B_0} = B_0\hat{y}$, and using the Ohm's law in the form $\overrightarrow{j} = \sigma(-\nabla\phi + \overrightarrow{u} \times \overrightarrow{B})$, Eq. (A.1) turns into:

$$\frac{\partial u}{\partial t} = -\frac{1}{\rho}\nabla p + \nu \left[\frac{\partial^2 u}{\partial y^2} + \frac{\partial^2 u}{\partial z^2}\right]$$
$$+ \sigma\frac{B_0}{\rho}\frac{\partial \phi}{\partial z} - \sigma\frac{B_0^2}{\rho}u \quad \text{(A.2)}$$

Now, combining $\nabla \cdot \overrightarrow{j} = 0$ with Ohm's law, one gets:

$$\frac{\partial^2 \phi}{\partial y^2} + \frac{\partial^2 \phi}{\partial z^2} - B_0\frac{\partial u}{\partial z} = 0 \quad \text{(A.3)}$$

Equations (A.2) and (A.3) constitute the system to solve in the gradient formulation. Next we define the dimensionless variables $\tilde{B} = B/B_0 = 1$, $\tilde{u} = u/u_0^*$, $\tilde{t} = \omega t$, $\tilde{y} = y/L$, $\tilde{z} = z/L$, $\tilde{d} = d/L$, $\partial\tilde{p}/\partial\tilde{x} = \tilde{G}e^{i\tilde{t}}$, ($\tilde{G}$ being the pressure gra-

dient amplitude). Dropping tildes and considering only dimensionless quantities from now on, they change into:

$$N_\omega^{-1}\frac{\partial u}{\partial t} = -\frac{\partial p}{\partial x} + M^{-2}\left[\frac{\partial^2 u}{\partial y^2} + \frac{\partial^2 u}{\partial z^2}\right] + \frac{\partial \phi}{\partial z} - u \quad \text{(A.4)}$$

$$\frac{\partial^2 \phi}{\partial y^2} + \frac{\partial^2 \phi}{\partial z^2} - \frac{\partial u}{\partial z} = 0 \quad \text{(A.5)}$$

Equations (A.4) and (A.5) would now constitute a restatement of the system to solve. Proposing $u = u_0(y,z)e^{it}$, and $\phi = \phi_0(y,z)e^{it}$, they conduce to a particularization of the problem for its spatial part as:

$$M^{-2}\left[\frac{\partial^2 u_0}{\partial y^2} + \frac{\partial^2 u_0}{\partial z^2}\right]$$

$$- \left(1 + iN_\omega^{-1}\right)u_0 = G - \frac{\partial \phi_0}{\partial z} \quad \text{(A.6)}$$

$$\frac{\partial^2 \phi_0}{\partial y^2} + \frac{\partial^2 \phi_0}{\partial z^2} - \frac{\partial u_0}{\partial z} = 0 \quad \text{(A.7)}$$

With spatial boundary conditions for isolating and perfectly conducting side and Hartmann walls (respectively) given by:

$$u_0(y = \pm a; z) = \phi_0(y = \pm a; z) = 0 \quad \text{(A.8)}$$

$$u_0(y; z = \pm 1) = \frac{\partial \phi_0}{\partial z}(y; z = \pm 1) = 0 \quad \text{(A.9)}$$

Equations (A.6) and (A.7) subject to boundary conditions given by Eqs. (A.8) and (A.9) can be solved by means of applying a suitable separation of variables. This begins by making ourselves sure that solutions for $u_0(y,z)$ and $\phi_0(y,z)$ in the following form satisfy the boundary conditions, given firstly by Eq. (A.9):

$$u_0(y,z) = \sum_{n=0}^{\infty} u_n(y)Cos(\alpha_n z) \quad \text{(A.10)}$$

$$\phi_0(y,z) = \sum_{n=0}^{\infty} \phi_n(y)Sin(\alpha_n z) \quad \text{(A.11)}$$

Indeed they do, once considering that:

$$G(z) = G\sum_{n=0}^{\infty} a_n Cos(\alpha_n z) \quad \text{(A.12)}$$

With $\alpha_n = (2n+1)\pi/2$, $a_n = {}^{4(-1)^n}/_{(2n+1)\pi}$, and $n = 0, 1, 2, 3, ...$

Replacing Eqs. (A.10) and (A.11) into (A.8) and (A.9), one obtains:

$$M^{-2}\frac{d^2 u_n(y)}{dy^2} - \left(M^{-2}\alpha_n^2 + \eta\right)u_n(y)$$

$$+ \alpha_n \phi_n(y) - Ga_n = 0 \quad \text{(A.13)}$$

$$\frac{d^2 \phi_n(y)}{dy^2} - \alpha_n^2 \phi_n(y) + \alpha_n u_n(y) = 0 \quad \text{(A.14)}$$

With $\eta = 1 + iN_\omega^{-1}$. This last ordinary differential equations system is subject to the following boundary conditions:

$$u_n(\pm a) = \phi_n(\pm a) = 0 \quad \text{(A.15)}$$

Solutions for the the system of Eqs. (A.13) and (A.14) subject to boundary conditions given by equations (A.15) take the form:

$$u_n(y) = \frac{\delta e^{-\frac{y(\sqrt{\epsilon_1}+\sqrt{\epsilon_2})}{\sqrt{2}}}}{8\pi\gamma(2n+1)\epsilon}\left(e^{\zeta_1 y}\left(4\epsilon e^{\zeta_2 y}((2n+1)\pi)^2 + \epsilon_1\left(((2n+1)\pi)^2 - 2\epsilon_2\right)\left(e^{\sqrt{2}y\sqrt{\epsilon_2}}+1\right)Sech(a\zeta_2)\right)\right.$$

$$\left. - \epsilon_2 e^{\zeta_2 y}\left(((2n+1)\pi)^2 - 2\epsilon_1\right)\left(e^{\sqrt{2}y\sqrt{\epsilon_1}}+1\right)Sech(a\zeta_1)\right) \quad \text{(A.16)}$$

$$\phi_n(y) = \frac{\delta}{2\gamma\epsilon}\left(2\epsilon - \epsilon_2 Sech(a\zeta_1)Cosh(\zeta_1 y) + \epsilon_1 Sech(a\zeta_2)Cosh(\zeta_2 y)\right) \quad \text{(A.17)}$$

With $\beta = \eta M^2 + \alpha_n^2$, $\gamma = (1-\eta)M^2\alpha_n^2 - \alpha_n^4$, $\delta = GM^2 a_n \alpha_n$, $\epsilon = \sqrt{\beta^2 + 4\gamma}$, $\epsilon_1 = \beta - \epsilon$, $\epsilon_2 = \beta + \epsilon$, $\zeta_1 = \sqrt{\epsilon_1}/\sqrt{2}$, and $\zeta_2 = \sqrt{\epsilon_2}/\sqrt{2}$. Final solutions are reconstructed by replacing solutions for $u_n(y)$ and $\phi_n(y)$ provided by Eqs. (A.16) and (A.17) into Eqs. (A.10) and (A.11) in order to find out $u_0(y,z)$ and $\phi_0(y,z)$. Once that's completed, one can put together $u = u_0(y,z)e^{it}$, $\phi = \phi_0(y,z)e^{it}$ as written in Eq. (34). Ultimately the velocity is normalized as proposed in Eq. (27) before visualization.

Acknowledgments

---

i. That is, j_{y0}, j_{z0} and j_{yow}, j_{z0w} only depend on y and z; being then two dimensional.

ii. In other words, due to symmetry over a quarter of the duct, the electric current within fluid and wall regions can be represented by electric current stream fluid and wall regions functions. In its turn, these can be expressed as potential fluid and wall regions functions which can then be decoupled via the thin wall approximation. The whole procedure ends with $F = F(y, z)$. Further details in [12,13].

1. Aysegül Akyüz and M. Sezer, *Applied Mathematics and Computation* **144** (2003) 237-247.

2. Aysegül Akyüz-Dascioglu and M. Sezer, *Journal of the Franklin Institute* **342** (2005) 688-701.

3. K. Barrett, *International Journal for Numerical Methods in Engineering* **50** (2001) 1893-1906.

4. C. Bozkaya and M. Tezer-Sezgin, *Journal of Computational and Applied Mathematics* **203** (2007) 125-144.

5. N. Bozkaya and M. Tezer-Sezgin, *Journal for Numerical Methods in Fluids*, **56** (2008) 1969-1991.

6. Ibrahim Çelik, *Applied Mathematics and Computation* **168** (2005) 125-134 .

7. Ibrahim Çelik, *Applied Mathematics and Computation* **160** (2005) 401-410 .

8. Ibrahim Çelik, *Applied Mathematics and Computation* **174** (2006) 910-920.

9. Ibrahim Çelik,. *International Journal for Numerical Methods in Fluids* **66** (2011) 1325-1340.

10. Ibrahim Çelik and Guzin Gokmen, *Applied Mathematics and Computation* **170** (2005) 285-295.

11. C. C. Chang and T. S. Lundgren, *Zeitschrift für Angewandte Mathematik und Physik ZAMP* **12** (1961) 100-114.

12. S. Cuevas, *Liquid-metal flow and heat transfer under strong magnetic fields. PhD thesis*, Facultad de Ciencias, Universidad Nacional Autónoma de México, (1994).

13. S. Cuevas, B.F. Picologlou, J.S. Walker, and G. Talmage, *International Journal of Engineering Science*, **35** (1997) 485-503.

14. M. Dehghan and D. Mirzaei, *Computer Physics Communications* **180** (2009) 1458-1466.

15. Z. Demendy and T. Nagy, *Acta Mechanica* **123** (1997) 135-149.

16. L. Gardner and G. Gardner, *Computer Methods in Applied Mechanics and Engineering* **124** (1995) 365-375.

17. J.C.R. Hunt, *Journal of Fluid Mechanics* **21** (1965) 577-590.

18. J.C.R. Hunt and K. Stewartson, *Journal of Fluid Mechanics* **23** (1965) 563-581.

19. Cenk Kesan, *Applied Mathematics and Computation* **134** (2003) 109-124.

20. Huan-Wen Liu and Song-Ping Zhu, *The Anziam Journal* **44** (2002) 305-322.

21. K. K. Mandal, *Applied Scientific Research* **19** (1968) 97-110.

22. K.K. Mandal, *Applied Scientific Research* **21** (1969) 1-12.

23. A. Mehmood and A. Ali, *Romanian Journal of Physics* **52** (2007) 85.

24. A. Neslituk and M. Tezer-Sezgin, *Computer Methods in Applied Mechanics and Engineering*, **194** (2005) 1201-1224.

25. A. Neslituk and M. Tezer-Sezgin, *Journal of Computational and Applied Mathematics*, **192** (2006) 339-352.

26. M. Sezer and M. Kaynak, *International Journal of Mathematical Education in Science and Technology*, **27** (1996) 607-618.

27. F. Shakeri and M. Dehghan, *Applied Numerical Mathematics*, **61** (2011) 1-23.

28. J.A. Shercliff, *In Mathematical Proceedings of the Cambridge Philosophical Society*, **49** (1953) 136-144.

29. B. Singh and P. Agarwal, *Zeitschrift für Angewandte Mathematik und Physik ZAMP*, **35** (1984) 760-770.

30. B. Singh and J. Lal, *Indian J. Pure Appl. Math*, **9** (1978) 101-115.

31. B. Singh and J. Lal, *Indian J. of Technology*, **17** (1979) 184-189.

32. B. Singh and J. Lal, *International Journal for Numerical Methods in Fluids*, **4** (1984) 291-302.

33. M. Tezer-Sezgin, *International Journal for Numerical Methods in Fluids*, **18** (1994) 937-952.

34. M. Tezer-Sezgin and S.H. Aydin, *Engineering Analysis with Boundary Elements* **30** (2006) 411-418.

35. M. Tezer-Sezgin and S. Köksal, *International Journal for Numerical Methods in Engineering* **28** (1989) 445-459.